Tunable light diffractor associated with liquid crystal molecular reorientation from homogeneous alignment to periodic twist deformation in micrometre scale

2011 J. Phys. D: Appl. Phys. 44 165501

(http://iopscience.iop.org/0022-3727/44/16/165501)

IOP PUBLISHING JOURNAL OF PHYSICS D: APPLIED PHYSICS

J. Phys. D: Appl. Phys. **44** (2011) 165501 (8pp) doi:10.1088/0022-3727/44/16/165501

Tunable light diffractor associated with liquid crystal molecular reorientation from homogeneous alignment to periodic twist deformation in micrometre scale

Surjya Sarathi Bhattacharyya[1], Dong Won Kwon[1], Young Jin Lim[1], Jae-Hyeung Park[2,3] and Seung Hee Lee[1,3]

[1] Department of BIN Fusion Technology and Department of Polymer-Nano Science and Technology, Chonbuk National University, Jeonju, Jeonbuk 561-756, Korea
[2] Department of Electrical and Computer Engineering, Chungbuk National University, Cheongju, Chungbuk 361-763, Korea

E-mail: jh.park@cbnu.ac.kr and lsh1@chonbuk.ac.kr

Received 17 December 2010, in final form 10 February 2011
Published 7 April 2011
Online at stacks.iop.org/JPhysD/44/165501

Abstract
We have demonstrated the formation of a transmissive tunable light diffractor with a fine grating period using a fringe-field switching (FFS) device. The presented device operates as a superposed amplitude and phase grating. The phase grating is formed by a thin slab of a nematic liquid crystal (LC) film and the amplitude grating is constructed by the electrode pattern of the FFS device. The electrode-position-dependent periodic deformation of the LC director as a function of the applied electric field is analysed and the respective occurrence of phase difference in monochromatic, coherent, linearly polarized He–Ne (632.8 nm) laser light is also calculated using the Jones matrix method at operating voltage. The same calculation results show that the transmitted beam of the present FFS diffractor is right-handed elliptically polarized. The operation characteristics of the thin diffracting device are investigated using a He–Ne laser source and a photodetector which shows a significantly large angular deviation of the diffracted beam owing to the small periodicity of LC deformation.

(Some figures in this article are in colour only in the electronic version)

1. Introduction

Tunable phase gratings have a wide range of applications. One of the important applications of a tunable phase grating is the newly developed super resolution microscopy technique [1–6] using structured illumination. The structured illumination technique [7, 8] achieves high resolution beyond the diffraction limit by projecting an amplitude grating pattern on the specimen, causing a beat pattern called moiré to appear. The spatial frequency of this moiré pattern is much smaller than that of the specimen, hence this moiré pattern can be easily observed in a microscope even if the features of the original specimen are too fine to resolve. In order to project the amplitude grating pattern on the specimen, a phase grating is usually used. The laser light is diffracted by a phase grating and two diffracted beams corresponding to +1 and −1 orders are refocused near the opposite edges of the back focal-plane aperture of the objective lens, generating an amplitude grating pattern by interference.

Transmission-type tunable phase gratings with a fine grating period can play a vital role in structured illumination techniques. The spatial frequency of the projected interference pattern should be large enough to bring high spatial frequency components of the specimen pattern into the limit of the numerical aperture (NA) of the objective lens. Since the spatial frequency of the projected interference pattern is determined by the diffraction angle of the phase grating, a fine grating period is required to produce a large diffraction angle and

[3] Authors to whom any correspondence should be addressed.

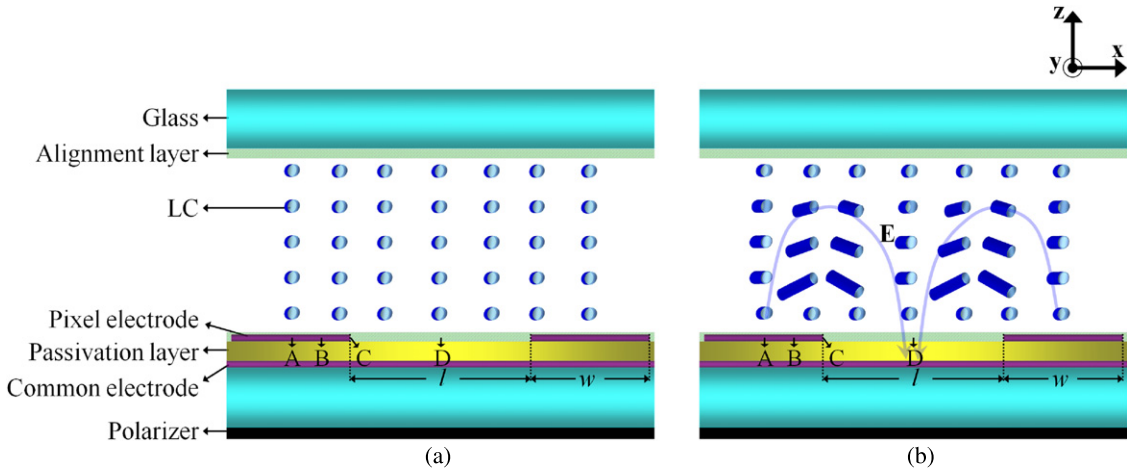

Figure 1. Schematic diagram of cell structure and configuration of LC molecules having positive dielectric anisotropy in the field off and field on states driven in FFS mode.

hence sufficient spatial frequency of the interference pattern. The tunability of the phase grating makes it possible to project different interference patterns without actually changing the optical system, making the system more stable and giving extra control over the image quality. Finally transmission-type structure simplifies the optical configuration.

In this paper we have discussed the operating principle of a newly devised transmission-type tunable light diffractor working as a superposed amplitude and phase grating with 5.0 μm grating period. The presented device uses a liquid crystal (LC) cell that exhibits a periodical change of LC orientation in the presence of a fringe electric field from homogeneously aligned LC state. The electrode structure of the LC device used here is the same as that in the fringe-field switching (FFS) device [9–13] acting as the amplitude grating. Considering the electrode structure of the FFS device, a plane-shaped common electrode is located below the slit-forming pixel electrode, with a passivation layer between the pixel and common electrodes, as shown in figure 1 [9]. Here, the pixel electrodes have a width (w) and are separated regularly by a distance (l). The LC molecules are homogeneously aligned above the pixel electrode in the initial state with their optic axis coinciding with the direction of polarized incident light. The fringe field generated by the present electrode structure has strong components in the horizontal (E_x) as well as vertical (E_z) directions, and as a result the LCs rotate above the whole electrode surface. The applied fringe electric field by the patterned electrode induces twist and tilt deformations (figure 1(b)) to the homogeneously aligned LC director (figure 1(a)). Interestingly, the field intensity periodically changes along the x-direction, and thus the distribution of twist and tilt angles of LC molecules has the same periodicity. Both the twist and tilt deformations induced over the LC director are tunable with the applied field and also show field reversibility. Hence, the present device can control the phase delay of the transmitting light passing through the LC layers. Thus, the control of intensity in different orders as a function of the applied field is possible with this device.

2. Experimental and simulation conditions

For preparing the FFS device, initially, a 40 nm thick indium tin oxide (ITO) coating is deposited on the transparent bottom glass substrate and then the SiO_2 passivation layer, with 690 nm thickness coated by chemical vapour deposition. Finally, a 40 nm thick second ITO layer is deposited and patterned as interdigital electrodes over the passivation layer. The width of the second ITO electrodes is 4 μm with a distance of 6 μm between electrodes. There is no electrode on the top glass substrate. In this case, the first and second ITO layers perform the role of a common electrode and a pixel electrode, respectively. There is no horizontal distance between the first and second ITO layers so that fringe-field lines are generated instead of generating the in-plane field as obtained in the case of interdigitated in-plane switching (IPS) mode with a bias voltage. The alignment layer AL-1051 purchased from Japan Synthetic Rubber Co. is coated on both substrates and the rubbing was performed in antiparallel directions. The rubbing angle (α) is defined as the angle made by the LC director with respect to the horizontal component of the fringe field and it is 83° in our case. The angle is chosen so as to have a sufficient deformation of the LC director. The pretilt angle generated by the rubbing is 3° but a lower value is favoured for an incident polarized light to experience a larger effective refractive index in the normal direction. The glass substrates are assembled to give a cell gap (d) of 4.1 μm. LC samples with positive dielectric anisotropy ($\Delta\varepsilon = 8.2$), ordinary refractive index (n_o) $\sim$ 1.4927 and extraordinary refractive index (n_e) $\sim$ 1.5917 having elastic constants $k_{11} = 9.7$, $k_{22} = 5.2$, $k_{33} = 13.3$ (pN) and rotational viscosity 80 mPa s purchased from Merck Co. are used in our experiments. The homogeneous alignment of the LC director and its electric-field-induced deformation are verified under a polarizing optical microscope (POM).

The experimental setup for studying the diffraction characteristics at room temperature consists of normally incident He–Ne laser ($\lambda = 633$ nm) light, followed by a pin hole, one sheet of polarizer, FFS cell and light detector.

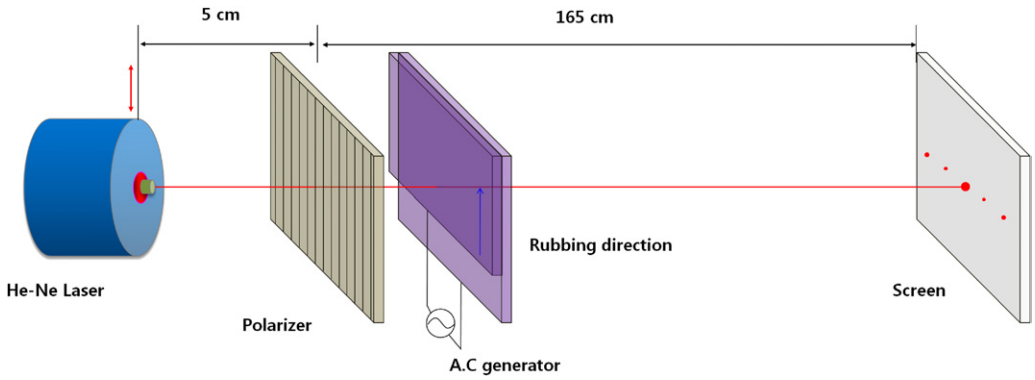

Figure 2. Schematic of the measurement setup for investigating the diffraction phenomenon occurring in the FFS device.

The experimental setup is shown schematically in figure 2. The pinhole is used to generate a point source which reduces overlapping in the diffracted beam. The polarizer sheet sets the direction of polarization of the incident light along the unbiased long axis of LC molecules (rubbing direction of the FFS device). The FFS device is driven with variable amplitude, 60 Hz square pulses from (Tektronix, AFG3022) a function generator. Finally, the intensity of the diffracted light is detected by a photodetector (Nanotek NLS-OP01).

The electro-optic characteristics of the FFS device are also analysed theoretically using the commercially available software 'LCD Master' (Shintech, Japan). In the simulation, two different kinds of energies are considered, namely the elastic energy and the electric energy. The LC director deformation can be explained in terms of splay, twist and bend deformations. The associated free energy density can be written in terms of the respective elastic constants such as k_{11}, k_{22} and k_{33}. Thus, the elastic free energy per unit volume (F_{elastic}) can be written as

$$F_{\text{elastic}} = \tfrac{1}{2}k_{11}(\nabla \cdot \hat{n})^2 + \tfrac{1}{2}k_{22}(\hat{n} \cdot \nabla \times \hat{n})^2 + \tfrac{1}{2}k_{33}\left(\hat{n} \times \nabla \times \hat{n}\right)^2. \quad (1)$$

For analytical studies it is useful to work in the approximation where the elastic constants are all equal. In that case, x, y and z components n_x, n_y, n_z of the director field $\hat{n}$ can be expressed as $n_x = \cos\theta \sin\psi$, $n_y = \sin\theta \sin\psi$ and $n_z = \cos\psi$, where θ and ψ represent the tilt and twist deformations, respectively. Equation (1) can now be written in the form

$$F_{\text{elastic}} = \tfrac{1}{2}k[(\nabla\psi)^2 + \sin^2\psi(\nabla\theta)^2 + 2\sin\psi\hat{n} \cdot (\nabla\theta \times \nabla\psi)]. \quad (2)$$

In the presence of electric field, the electric free energy F_{electric} per unit volume is given by

$$F_{\text{electric}} = -\tfrac{1}{2}\varepsilon_0\Delta\varepsilon(\vec{E} \cdot \hat{n})^2 \quad (3)$$

where $\vec{E}$ is the applied electric field. Then the total free energy per unit volume is given by

$$F = F_{\text{elastic}} + F_{\text{electric}}. \quad (4)$$

The LC director distribution is calculated by minimizing the above free energy equation. The optical calculation is based on the 2×2 extended Jones matrix [14] using the initial conditions identical to those of experiments.

3. Results and discussion

To analyse the electro-optic characteristics of the new device, we have calculated the LC director configuration and electrode-position-dependent transmittance with the variation of applied voltage at 0% (0 V), 25% (1.8 V), 50% (2.2 V), 75% (2.6 V) and 100% (4.2 V) of transmission levels in the transmissive FFS device. For different applied voltages the director configuration is depicted in figure 3. These are the voltages usually considered in LCDs and near the maximum voltage for the said device operation the LC reorientation is sufficiently stable. Hence both simulations as well as experiments are limited to the maximum voltage for device operation ($V_{\text{op}} =$ 4.2 V). The results are obtained from simulations and also verified experimentally by voltage-dependent transmittance curves for the constructed FFS device. The simulation results are obtained with identical initial conditions as those of experiments. We label A, B, C and D as positions at the centre, between the edge and the centre, the edge of the pixel electrodes and middle of consecutive electrodes, respectively. It is evident from the simulated director configuration of the LC molecule that the applied electric field in the FFS device generates both horizontal (E_x) as well as vertical (E_z) field components. Hence the said LC molecules show tilt and twist deformations. The deformations are found to be electrode-position-dependent and periodic. Both tilt and twist deformations are found to increase with increasing amplitude of applied voltage as in figures 3(*a*), (*b*) and (*c*). Consequently, the maximum transmittance increases, though it also shows periodic crests and troughs along the electrode position. Since the transmittance profile obtained from the simulation between the centres to the edge of the pixel electrode is repeatable, it can represent the characteristic of the whole device transmittance. The LC director profile at the mentioned distance has to be well understood to obtain the reason behind the resultant light modulation by the device. The LC director profile obtained from the simulation leads us to the fact that LC is twisted first by a strong dielectric torque ($\Gamma_{\text{dielectric}}$) between E_x and the LC director $\hat{n}$ at the electrode edge (about position C). With increasing magnitude of applied field the additional tilt deformation symmetrically appears on either side of the electrode edge. It is worth mentioning here that the symmetry of the electric lines of forces from

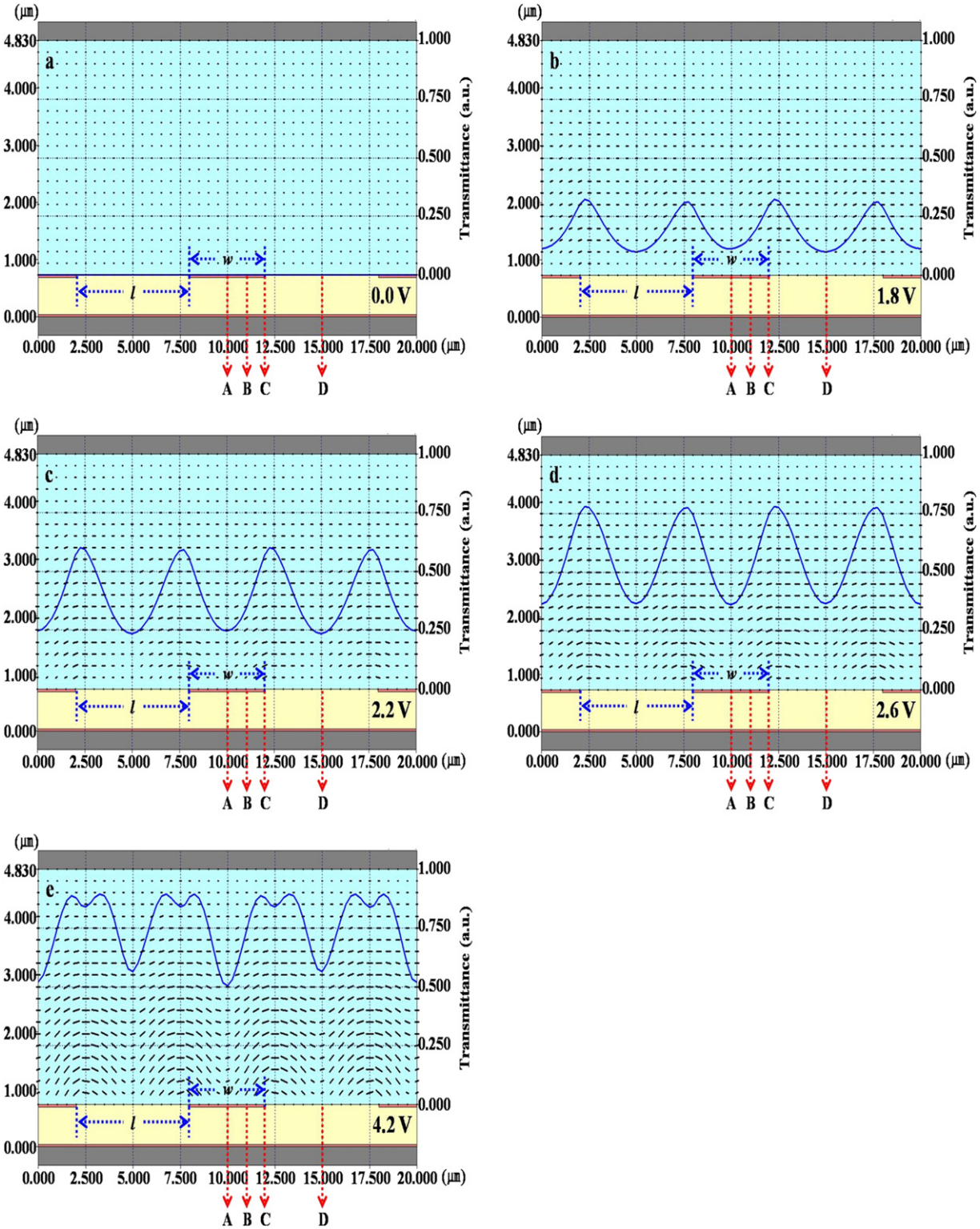

Figure 3. Distribution of LC molecules and corresponding transmittance (continuous line) as a function of applied voltage of magnitude 0 V (*a*), 1.8 V (*b*), 2.2 V (*c*), 2.6 V (*d*) and 4.2 V (*e*) transforming from dark to bright state of the FFS mode at transmission levels 0%, 25%, 50%, 75% and 100%, respectively, using a positive dielectric anisotropic LC.

the pixel electrode to the common electrode is reflected in the director configuration of our positive dielectric anisotropic sample. Least deformation of the LC director is found at the centre of the pixel and at the middle of the consecutive pixels due to minimal dielectric torque in those regions. The said regions show twist deformation at the optimal value of applied voltage (4.2 V), due to the twisting elastic force supplied by neighbouring molecules. Consequently, in FFS mode $\Gamma_{\text{dielectric}}$ and Γ_{elastic} have a switching role depending on the horizontal position. However, according to earlier discussion $\Gamma_{\text{dielectric}}$ leads to Γ_{elastic}, and hence the deformation of LC starts from the pixel edges and then spreads towards the central regime with

increasing applied field strength. The total bulk torque Γ_{total} per unit volume needed to distort the LCs in a homogeneously aligned state in the FFS device can be described as

$$\vec{\Gamma}_{\text{total}} = \vec{\Gamma}_{\text{elastic}} + \vec{\Gamma}_{\text{dielectric}}$$
$$= \sum \left(\frac{\partial F_{\text{elastic}}}{\partial \theta} + \frac{\partial F_{\text{elastic}}}{\partial \psi} \right) + \Delta\varepsilon(\vec{E}.\hat{n})(\vec{E} \times \hat{n}) \qquad (5)$$

where θ and ψ are the dynamical variables representing tilt and twist deformations, respectively.

According to earlier discussion when the applied field is considerably smaller than V_{op}, the LC director shows very small deformation in regions A and C, whereas the deformation is much larger in B and D regimes. This fact also resembles the simulated transmittance results as the edge and between regimes transmit much more than the middle regime. Here we assume that the LC molecules are parallel to the substrate in the initial state with no external field with a small pretilt of 3°. Linearly polarized light along the optic axis of LCs will then experience an extraordinary refractive index (n_{e}). As the electric field is applied, the LC molecules tilt and the refractive index changes periodically closer to the edge regime. If the applied field is strong enough the LC will be homeotropic and the incident light will experience an ordinary refractive index. In the presence of applied electric field the deformed LC layers are assumed to act as a series of retardation plates to the polarized monochromatic incident laser beam. Hence, using the LC director orientation information obtained from simulation results, we have determined the phase retardation as well as polarization state of the output beam at every electrode position. We have used the Jones matrix formalism [15] in the above-mentioned process.

The Jones vector of the incident light beam for each layer of LC in the most general form is expressed as

$$\tilde{A} = \begin{pmatrix} A_{0x} e^{i\varphi_x} \\ A_{0y} e^{i\varphi_y} \end{pmatrix} \qquad (6)$$

where A_{0x} and A_{0y} represents the amplitudes, and φ_x and φ_y represents the respective phases of the horizontal and vertical components of the incident beam. Similarly, considering the tilt and twist deformations of the successive LC layers we have determined the Jones vector of the output beam as shown:

$$\tilde{A}' = \begin{pmatrix} \text{Cos}\psi & -\text{Sin}\psi \\ \text{Sin}\psi & \text{Cos}\psi \end{pmatrix} \begin{pmatrix} e^{-i\Gamma/2} & 0 \\ 0 & e^{i\Gamma/2} \end{pmatrix}$$
$$\times \begin{pmatrix} \text{Cos}\psi & \text{Sin}\psi \\ -\text{Sin}\psi & \text{Cos}\psi \end{pmatrix} \begin{pmatrix} A_{0x} e^{i\varphi_x} \\ A_{0y} e^{i\varphi_y} \end{pmatrix} = \begin{pmatrix} A'_{0x} e^{i\varphi'_x} \\ A'_{0y} e^{i\varphi'_y} \end{pmatrix} \qquad (7)$$

where ψ represents the twist deformation, Γ represents the phase retardation of the respective LC layers, and the amplitudes and phases of the horizontal and vertical components of the output beam are represented by A'_{0x}, φ'_x and A'_{0y}, φ'_y respectively. The phase retardation for each LC layer is given by

$$\Gamma = \frac{2\pi}{\lambda}(n_{\text{eff}} - n_{\text{o}})d \qquad (8)$$

where λ is the wavelength of the incident laser beam, d is the respective LC layer thickness, n_{o} is the ordinary refractive index of the used LC material and n_{eff} represents the effective refractive index of the incident laser beam for deformed LC layers and is depicted by

$$n_{\text{eff}} = \frac{n_{\text{o}} n_{\text{e}}}{\sqrt{n_{\text{o}}^2 \cos^2\theta(z) + n_{\text{e}}^2 \sin^2\theta(z)}} \qquad (9)$$

where $\theta(z)$ represents the tilt deformation as obtained from simulation.

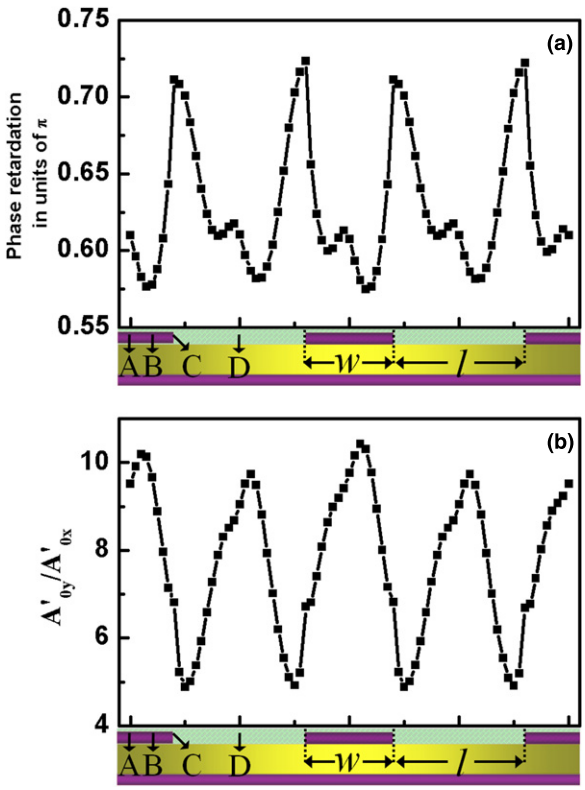

Figure 4. The profile of (*a*) phase retardation and (*b*) amplitude ratio for transmitted monochromatic coherent He–Ne laser (632.8 nm) light polarized incident along the rubbing direction as a function of horizontal electrode position at V_{op} following the Jones matrix method.

Figure 4 shows the calculated phase retardation and ratio of amplitudes of the horizontal and vertical components of the transmitted wave profile for monochromic coherent He–Ne laser light (632.8 nm) polarized along the rubbing direction as a function of horizontal electrode position at V_{op}. Interestingly, figure 4(*a*) shows the periodic phase fluctuation of ∼0.42 rad (0.13π) for every ∼5.0 μm horizontal separation. The phase retardation is peaked near the edge of the pixel electrodes and shows a dip near the middle of the successive pixels and the centre of the pixel regions. The electrode-position-dependent modulation of the ratio of amplitudes of the transmitted light (figure 4(*b*)) is found to be greater than one for all electrode positions. Also the magnitude of phase retardation is found to show a much lesser value than 1.57 rad (0.5π). Considering the relative signs of the respective phases of the horizontal and vertical components of the output beam, the transmitted light is found to be right-handed elliptically polarized for all electrode positions. However, the eccentricity of the ellipse is

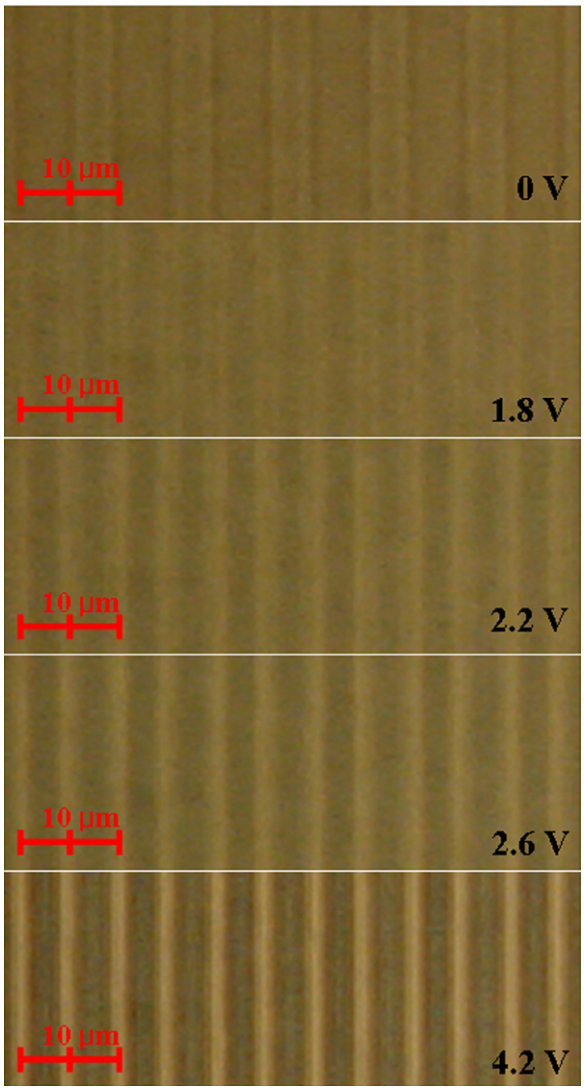

Figure 5. Optical microscopic textures of the FFS cell under parallel polarizers with increasing voltage, showing periodic dark and bright states.

found to vary periodically from the centre to the edge of the periodic pixel structure. To be more specific, the eccentricity is lower near the middle of the successive pixels and centre of the pixel regions and higher near the edges of the pixel electrodes. The boundary of phase fluctuation is sharp as shown in figure 4(*a*). The periodic phase modulation of the transmitted light through the FFS device leads to the formation of multiple beam interference as experimentally observed and discussed in the following text.

Figure 5 shows the microphotographs of the cell with a variation of applied external ac electric field strength from 0, 1.8, 2.2, 2.6 to 4.2 V under a parallel polarizer, for direct experimental verification of the periodic deformation of LC molecules. The FFS cell shows the electrode pattern in the absence of applied voltage. However, periodic striped deformation of the LC becomes more and more prominent by gradually raising the voltage. The transmittance at the centre of the pixel and common electrode is found to be consistently low as expected from our earlier discussion. In the low-field regime, the dielectric torque dominates the pixel edges and forces the LC molecules to twist as well as tilt and allows the device to start transmission from the edge regime. As we keep on increasing the applied field this effect becomes more intense, enhancing transmittance of the entire cell. However, the centre of the pixel and the middle of consecutive electrode remain dark. Hence the driving scheme generates a periodic bright and dark patterned grating. A careful analysis of the captured images using I. Solution software reveals that the periodic dark regions have a periodicity of $\sim 5\,\mu$m which is consistent with other investigations.

Now it is customary to refer the operation regime of the proposed grating. There are two well-known grating types, namely Raman–Nath and Bragg distinguished as thin and thick gratings, respectively [16]. The parameter Q that determines the criterion is given by

$$Q = \frac{2\pi\lambda_0 L}{\Lambda^2 n_{\mathrm{m}}} \tag{10}$$

where λ_0 is the wavelength of light, L is the grating thickness, Λ is the grating period and n_{m} is the mean refractive index. A 'thick' grating with $Q \gg 1$ corresponds to Bragg diffraction and can produce a strong diffraction maximum when the incident angle satisfies the phase matching condition. Here and below we measure all the angles (θ_m) with respect to the normal to the cell. For a 'thin' grating $Q \ll 1$, and is known as Raman–Nath diffraction. For normal incidence, the directions of the diffraction orders $m = 0; \pm 1; \pm 2 \ldots$

$$\theta_m = \arcsin(m\lambda/\Lambda). \tag{11}$$

In our experiment, Λ is found to be $\sim 9.9\,\mu$m for the odd orders and $\sim 4.9\,\mu$m for the even orders. The obtained magnitude of $Q \ll 1$ ensures that the grating belongs to the thin or Raman–Nath regime.

Figure 6 shows the images of the diffraction patterns obtained by the previously mentioned experimental arrangement. We have monitored the changes in diffraction pattern by varying the amplitude of the applied ac field. We recorded diffraction patterns by taking photographs of a screen placed 165 cm away from the tunable diffracting device. The change in intensity of the diffracted spots can be realized from the figure. The intensity of first-order diffraction in the absence of an applied voltage is found to be $\sim 2.8\,\mu$W which goes up to $14\,\mu$W at 4.2 V. The intensity of third-order diffraction is $\sim 1.9\,\mu$W under field off condition and it goes up to $5.7\,\mu$W, at 4.2 V. However, the second-order spot shows $1.7\,\mu$W intensity in the absence of an applied field, which goes up to $67\,\mu$W, at 4.2 V. Hence it is evident that the second-order diffraction beam becomes more intense as we keep on increasing the applied field.

The angles of diffraction in different orders in field off and field on (applying operating voltage of 4.2 V) are shown in table 1. The pinhole working as a non-ideal point source (width of the pinhole $\sim 100\,\mu$m) is responsible for finite width. The effects of amplitude as well as phase gratings are analysed in detail in the subsequent discussion.

A powermeter is placed over the screen for measuring the intensity of diffracted light. The powermeter's output

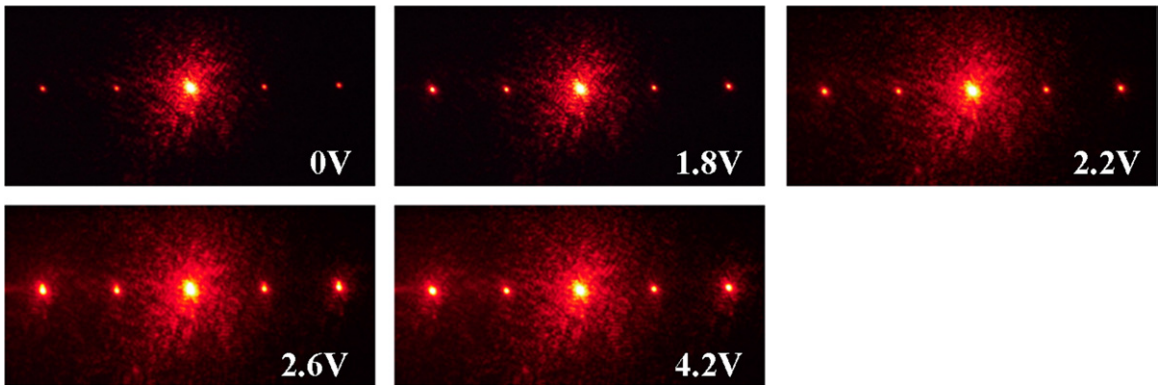

Figure 6. Photographs of diffraction pattern obtained from the constructed grating.

Table 1. Angle of diffraction in the field on and field off states observed for the tunable FFS diffractor.

Order of diffraction	Angle of diffraction (°)
Zeroth order	0
First order	3.68
Second order	7.37
Third order	11.10

is recorded with a variation of applied electric field. The intensity profiles for different diffraction orders with a variation of applied field are shown in figure 7. These profiles are symmetric on either side of the origin, where the transmitted light (zeroth-order diffraction) is set to appear. From this measurement it is clear that the intensity of the transmitted light decreases with increasing applied field. Significant enhancement of intensity of diffracted beam is observed for the even order diffracted beam with increasing magnitude of applied ac field; however, it is much weaker for the odd orders. Interestingly, the pixel structure of the FFS device has a periodicity of $\sim$10 μm, which almost coincides with the calculated magnitude of 'Λ', in accordance with equation (11), for first-order diffraction in the absence of applied field (0 V). The angular deviation for the higher order diffracted beams can also be matched using the same equation (equation (11)) owing to the same periodicity. However, the diffraction effect obtained from the amplitude grating (pixel structure) is not electrically tunable; hence it contributes to all diffracted spots in respective intensity, as obtained in the absence of applied field (0 V). This demand is supported by the image of laser diffraction shown in figure 6, as a clear diffraction pattern is obtained at the same angles even in the absence of an applied electric field. Hence, all the diffraction maxima are contributed by multiple beam diffraction from the electrode pattern having a periodicity of 10 μm and independent of the applied field.

However, we have also obtained electric-field-induced modulation in intensity of diffraction maxima, which is caused by field-induced modulation of the phase profile for monochromatic, coherent, He–Ne laser light passing through periodically distorted LC layers which forms the phase grating. It has to be mentioned that the demand for phase-modulated grating is also supported by the calculated phase modulation profile of LC (figure 4) having periodicity $\sim$5.0 μm, which coincides with the magnitude of 'Λ', obtained from the laser diffraction experiment in accordance with equation (11). Additionally, the electric-field-induced intensity modulation of the second-order diffraction beam is found to be stronger than that of other orders (figure 7). It is also noticeable from the figure that the diffraction efficiency of the device is not quite high; however, further improvement is possible using higher birefringence LC materials and by optimizing the periodic phase retardation conditions. The existence of electrode patterns only on one of the two substrate plates of the cell eliminates the possibility of anomalous LC distortion by cross-connecting field line orientation between the pixel and common electrodes.

4. Summary

In this paper we have highlighted the diffraction capability of a novel FFS device. Superposed effect of anisotropic phase grating and amplitude grating is demonstrated by driving a thin layer of a nematic liquid crystal film in FFS mode. The electric-field-induced LC director modulation and transmission characteristics of the device are estimated as a function of electrode position using a simulation software. The periodic phase retardation profile for monochromatic, coherent, linearly polarized He–Ne (632.8 nm) laser light is calculated using the Jones matrix method and also the polarization states of the output beam are determined for all electrode positions at V_{op}. The operation characteristics of the thin diffracting device are investigated using a He–Ne Laser source and a photodetector showing a significantly large angular deviation of the diffracted beam owing to the small periodicity of LC deformation. The periodicity also matches in POM image observations and electrode-position-dependent phase profile calculations. The electrically controllable intensity of different orders of a diffracted beam has potential applications in super resolution microscopy. Further research work is in progress to improve the efficiency of this potential device.

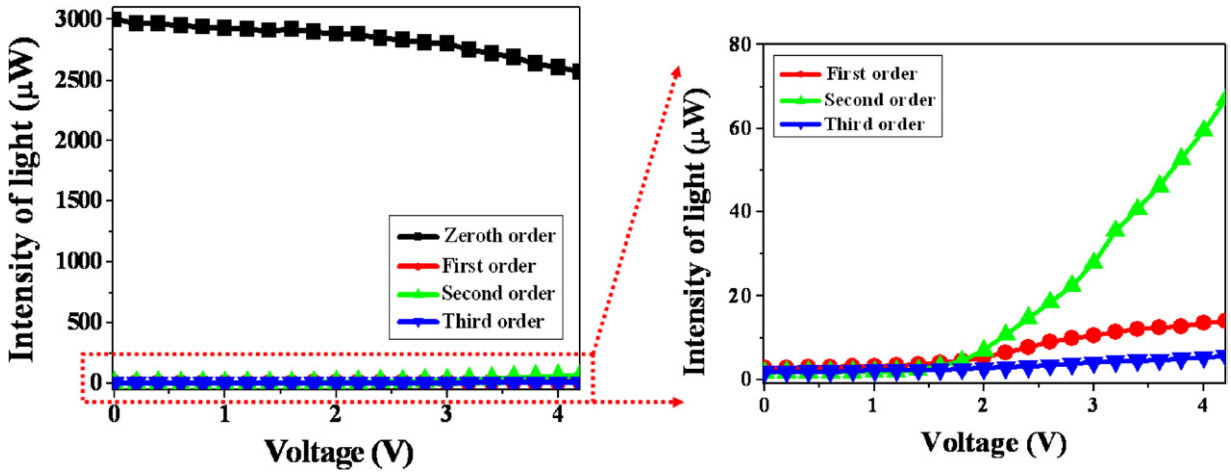

Figure 7. Measured intensity of diffracted He–Ne (632.8 nm) laser beam as a function of applied voltage to the homogeneously aligned FFS device.

Acknowledgments

The authors are grateful to the WCU program through MEST (R31-2008-000-20029-0) for financial support.

References

[1] Hell S W and Wichmann J 1994 *Opt. Lett.* **19** 780
[2] Klar T A and Hell S W 1999 *Opt. Lett.* **24** 954
[3] Hell S W and Kroug M 1995 *Appl. Phys.* B **60** 495
[4] Bretschneider S, Eggeling C and Hell S W 2007 *Phys. Rev. Lett.* **98** 218103
[5] Betzig E, Patterson G H, Sougrat R, Lindwasser O W, Olenych S, Bonifacino J S, Davidson M W, Schwartz J L and Hess H F 2006 *Science* **313** 1642
[6] Rust M J, Bates M and Zhuang X 2006 *Nature Methods* **3** 793
[7] Gustafsson M G L 2005 *Proc. Natl Acad. Sci. USA* **102** 13081
[8] Gustafsson M G L 2000 *J. Microsc.* **198** 82
[9] Lee S H, Lee S L and Kim H Y 1998 *Appl. Phys. Lett.* **73** 2881
[10] Jung S H, Kim H, Song S, Kim J-H, Nam S-H and Lee S H 2004 *Japan. J. Appl. Phys.* **43** 1028
[11] Noh J-D, Kim H Y, Kim J-H, Nam S-H and Lee S H 2003 *Japan. J. Appl. Phys.* **42** 1290
[12] Ryu J W, Lee J Y, Kim H Y, Park J W, Lee G-D and Lee S H 2008 *Liq. Cryst.* **35** 407
[13] Lim Y J, Kim J H, Her J H, Park K H, Lee J H, Kim B K, Kang W-S, Lee G-D and Lee S H 2010 *J. Phys. D: Appl. Phys.* **43** 085501
[14] Lien A 1990 *Appl. Phys. Lett.* **57** 2767
[15] Yeh P and Gu C 1999 *Optics of Liquid Crystal Displays* 2nd edn (New York: Wiley)
[16] Klein W R and Cook B D 1967 *IEEE Trans. Sonics Ultras.* **SU-14** 123